Sensorless control of IM based on stator-voltage MRAS for Limp-home EV applications

Ehsan Dehghan-Azad (corresponding author**), Shady Gadoue, and David Atkinson**

School of Electrical and Electronic Engineering, Newcastle University, Newcastle Upon-Tyne, NE1 7RU, UK. (email: e.dehghan-azad@newcastle.ac.uk; shady.gadoue@ncl.ac.uk; dave.atkinson@ncl.ac.uk)

Howard Slater, and Peter Barrass

Sevcon Ltd. Gateshead, NE11 0QA, UK. (email: howard.slater@sevcon.com; peter.barrass@sevcon.com)

Frede Blaabjerg

The Institute of Energy Technology, Aalborg University, Pontoppidanstraede 101, Aalborg, DK-9220, Denmark. (email: fbl@et.aau.dk)

Abstract— This paper proposes a novel sensorless speed estimation for an induction motor (IM) based on a new stator voltage model reference adaptive system (Vs-MRAS) scheme. This is utilized for torque-controlled drive (TCD) based on indirect rotor field oriented control (IRFOC) technique in *limp-home* mode operation of EV applications. The Vs-MRAS scheme uses the error between the reference and estimated stator voltage vectors and estimates the synchronous speed. Unlike existing MRAS schemes, the proposed sensorless scheme does not require the measured nominal values of stator resistance, stator inductance, and rotor resistance. This scheme is insensitive to variations of the aforementioned parameters. Moreover, using the proposed scheme eliminates the need for slip calculation. The proposed scheme is implemented and experimentally tested in a lab environment, on a 19-kW IM**,** and also applied on an electric golf buggy, powered by a 5-kW IM. The experimental results show that the proposed scheme is immune to parameter variations and is consistent in vehicle-starting from standstill and hill-starting tests. This scheme is also free from drift problems associated with a pure integration and is stable in the field weakening region. The test-drive results from the golf buggy confirm suitability of the proposed Vs-MRAS scheme over a wide range of speeds for the purpose of TCD in EV applications.

Index Terms— Electric Vehicle, Induction Motor, Torque Controlled Drive, Field Oriented Control, Sensorless, Model Reference Adaptive System.

I. INTRODUCTION

Recent increase in the popularity of Electric Vehicles (EV) has prompted researchers to concentrate more on fault tolerant drives (FTDs). The FTD concept improves safety, reliability and availability of EVs [1]. This concept simply means that the drive will continue to function in a satisfactory manner regardless of fault occurrence [2]. One of the highly scoring critical safety issues in the Fault Modes and Effect Analysis (FMEA) of EV, is speed/position sensor failure during drive. This fault can immobilize the electrical motor drive mechanism and bring the EV to halt mode. Despite the fact that the likelihood of the speed/position sensor failure is small or has low level of exposure classification in the Automotive Safety Integrity Level (ASIL), it has significant high scores in the severity and controllability classifications. Occurrence of this failure on a high-way or a crowded roundabout can lead to life-threatening events. Therefore in order to comply with the road vehicles-functional safety standards (ISO26262), it is critically important for the drive mechanism employed for EV applications to be fault tolerant against the speed/position sensor. The FTD mechanism may have degraded level of performance after sustaining the fault [3], but it would permit driver and passengers of EVs to reach their destination safely despite sensor failure, this is known as *limp-home* mode. The limp-home mode concept consists of three parts, which are; fast fault detection, smooth transition between sensor-ed to sensorless and vice versa, and more importantly a robust sensorless speed estimator. The latter is of high importance and will only be focused on in this paper. The first two parts are outside of the scope of this paper and have already been dealt with by Chakraborty and Verma [4]. For EV applications torque controlled drive (TCD) of induction motor (IM) is normally used [5]. In the absence of a mechanical sensor, TCD based on indirect rotor field oriented control (IRFOC) requires sensorless speed estimation for rotor flux angle calculation.

In the past years, several sensorless speed estimation schemes have been proposed for IM in literature [6-14].These are; Extended Kalman Filter (EKF) [7, 8], Sliding Mode Observer (SMO) [11]. Adaptive Full-order Observer (AFO) [9, 10]. Model Reference Adaptive System (MRAS) schemes [6, 13, 14], Neural Networking (NN) [12]. It is essential for the sensorless scheme which is employed, for the purpose of fault tolerant EV application, to be capable of functioning during vehicle-starting from standstill and low speeds. More importantly, the sensorless algorithm should be less complicated and require smaller execution time to make an efficient use of the limited available space in the Digital Signal Processor (DSP) [15]. Among these approaches, speed estimation based on MRAS schemes are relatively simpler to implement and often require lower computational effort [16, 17]. MRAS schemes, which have been developed so far in literature, can be divided according to how the error signal is calculated. These are; Rotor-flux (RF-MRAS) [18], back-electromotive-force (back-EMF MRAS) [19, 20], reactive-power (RP-MRAS) [6, 19], and stator current (CC-MRAS) [21]. Disadvantages of the RF-MRAS scheme

are; this scheme suffers from pure integration and is sensitive to the stator resistance variation [6, 13]. The back-EMF MRAS scheme was introduced to overcome problems associated with pure integration [19]. However, this scheme suffers from stator resistance variation [6] and is more difficult to design its adaptation gain constants [22]. Although the RP-MRAS scheme is immune to stator resistance variation, this scheme suffers from lack of stability in regenerating mode and shows low noise immunity [12, 20]. In order to overcome shortcomings related to sensitivity to parameter variations and issues related to stability, in the mentioned MRAS schemes, the CC-MRAS was proposed by [23]. This scheme takes the measured stator current components of the IM in the stationary reference frame as a reference system. The adjustable model calculates the estimated stator current components using the stator voltage and current models. However, in this scheme rotor flux estimation is required in order to estimate the stator current components. Therefore implementing this scheme increases complexity and requires more computational effort in comparison to other MRAS schemes. In the case of EV applications, where high computational effort is already required to execute various functional safety programmes, which is a critical aspect, implementing this scheme can become problematic.

In this paper, a novel stator voltage based MRAS (Vs-MRAS) scheme is proposed for the purpose of fault tolerant *limp-home* operation for EV applications. The proposed scheme takes advantage of stator voltage reference components in the stationary reference frame by setting them as its reference model. These are compared with the estimated stator voltage components using the measured stator current components. This scheme is computationally simpler to implement and is independent from the initially measured nominal motor parameters such as; stator resistance, stator inductance, and rotor resistance. The proposed scheme is immune to parameter variations, inverter nonlinearities, and errors due to digitization in the field weakening region. Experimental tests, based on a 19-kW IM and later on an electric golf buggy (powered with 5-kW IM), are carried out to investigate the performance of the proposed scheme. Experimental results show robustness of this scheme against stator resistance variation in addition to successful starting from standstill. The vehicle test–drive, utilizing the proposed scheme, confirms the consistency and reliability of this scheme in a wide speed range.

The structure of this paper is as follows; Section II describes sensorless TCD using IRFOC and a review of the fundamental concept of the conventional back-EMF MRAS scheme. Section III gives a detailed description of the new Vs-MRAS scheme. Section IV describes the experimental system platform and Section V shows the experimental results of the proposed sensorless scheme. Finally the conclusion is provided in Section VI.

II. SENSORLESS TORQUE CONTROLLED DRIVE

A. Torque controlled drive based on IRFOC technique

The Overall block diagram of the TCD based on IRFOC used in this paper is shown in Fig. 1. The accelerator pedal is used for applying the torque demand in EV by the driver. Several TCD approaches have been presented in literature [24-26]. Although these have different structures, in most cases an outer estimated torque/speed feedback loop is employed. Since correct rotor direction to that requested at the vehicle-starting from standstill is highly important for EV applications, eliminating the outer loop will reduce any uncertainties associated with the estimated signal in vehicle-starting from standstill and helps the rotor to go in the selected direction. Thus by utilizing a lookup table (LUT) to produce the value of d-axis stator current reference, q-axis stator current reference can be calculated by rearranging the electromagnetic torque equation

$$i_q^* = \frac{L_r\, T^*}{L_m^2 1.5 P i_d^*}. \tag{1}$$

Where; T^* is applied electromagnetic torque command. i_q^* and i_d^* are stator current components in the synchronous reference frame. P is pole pair, L_r and L_m are rotor and magnetizing inductances, respectively.

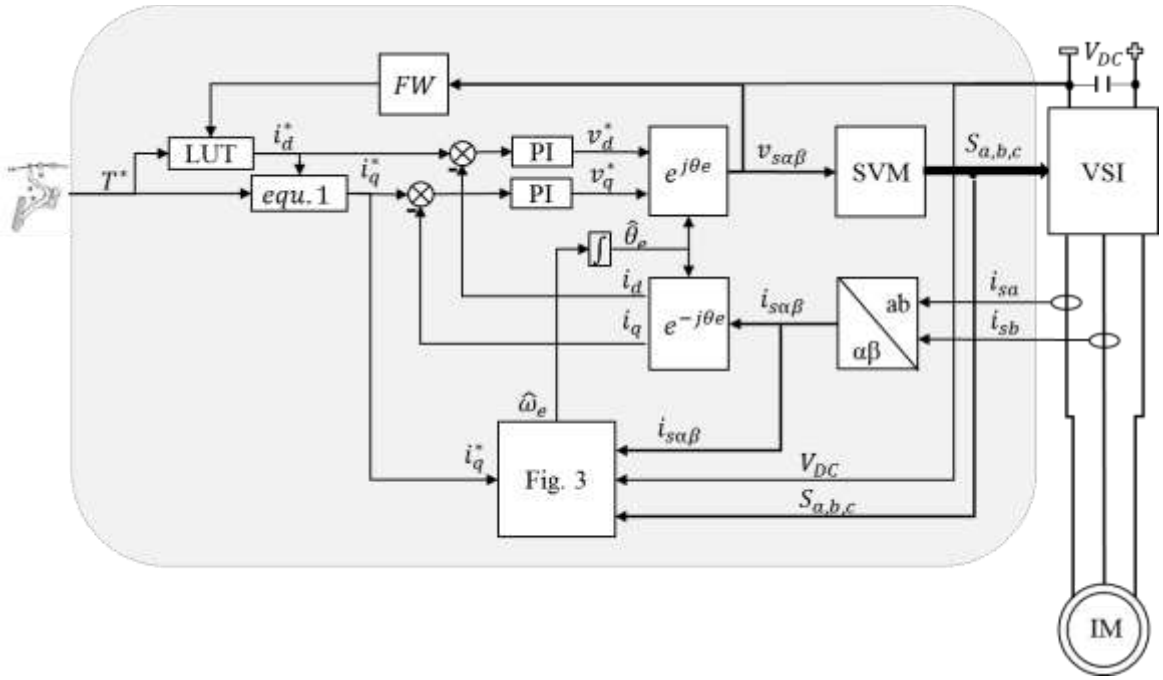

Fig. 1. The overall block diagram of the sensorless TCD of IM based on IRFOC for the purpose of EV application.

B. Conventional Back-EMF MRAS

The block diagram of the conventional back-EMF MRAS scheme is shown in Fig. 2. This includes a reference model, an adjustable model and an adaptation mechanism. The reference model is based on the voltage model of

IM in the stationary reference frame. It takes in stator voltage and current components and in return calculates back-EMF reference components. This can be shown by rearranging the IM stator voltage in the stationary reference frame [19].

$$\bar{e}_{m\alpha\beta} = \bar{v}_{s\alpha\beta} - (R_s + L_s\sigma p)\bar{\imath}_{s\alpha\beta}. \tag{2}$$

Where; ($\bar{e}_{m\alpha\beta} = e_{m\alpha} + je_{m\beta}$) is the reference back-EMF vector in the stationary reference frame. $\bar{v}_{s\alpha\beta}$ and $\bar{\imath}_{s\alpha\beta}$ are stator voltage and current vectors in the stationary reference frame, respectively. R_s and L_s are stator resistance and inductance, $p = \frac{d}{dt}$ is the differential operator, and $\sigma = 1 - (\frac{L_m^2}{L_s L_r})$ is the leakage coefficient.

The adjustable model takes in the stator current components and the estimated electrical rotor speed and in return provides two estimated back-EMF components. The estimated back-EMF vector output of the adjustable model in the stationary reference frame is given as [19].

$$\bar{\hat{e}}_{m\alpha\beta} = \frac{L_m}{L_r} p\bar{\psi}_{r\alpha\beta} = \frac{L_m}{L_r} \frac{(L_m\bar{\imath}_{s\alpha\beta} - \bar{\psi}_{r\alpha\beta} + j\hat{\omega}_r T_r\bar{\psi}_{r\alpha\beta})}{T_r}. \tag{3}$$

Where, ($\bar{\hat{e}}_{m\alpha\beta} = \hat{e}_{m\alpha} + j\hat{e}_{m\beta}$) is the estimated back-EMF vector in the stationary reference frame, $T_r = \frac{L_r}{R_r}$ is the rotor time constant (R_r is the rotor resistance), and $\hat{\omega}_r$ is the estimated electrical rotor speed.

The adaptation mechanism of MRAS schemes are designed based on Hyperstability concept [18, 19]. This concept allows the equations of the state error of MRAS to be asymptotically stable. The estimated electrical rotor speed is obtained from the output of a PI controller (adaptation mechanism).

$$\hat{\omega}_r = \left(k_p + \frac{K_i}{s}\right) * \left(\bar{\hat{e}}_{m\alpha\beta} \otimes \bar{e}_{m\alpha\beta}\right). \tag{4}$$

Where; k_p and K_i are proportional and integral gains, respectively, and $\otimes$ is the cross product sign.

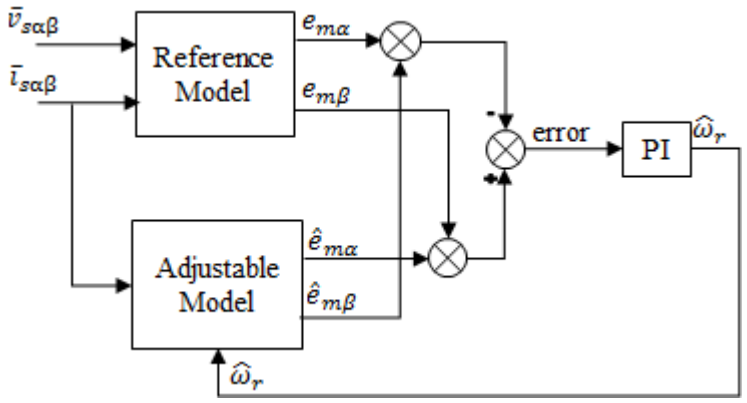

Fig. 2. Block diagram of the conventional back-EMF MRAS scheme.

III. PROPOSED STATOR VOLTAGE BASED MRAS SCHEME

The block diagram of the proposed Vs-MRAS scheme is shown in Fig. 3. The signal flow diagrams of the reference model, which is shown in the Fig 4, takes in the reconstructed and estimated (from the adjustable model output) stator voltage components in the stationary reference frame and in return provides the reference stator voltage components. The reference model takes advantage of two identical compensating mechanisms, similar to the one presented in [15]. Utilizing these compensators make the proposed scheme immune to errors which are due to parameter variations, inverter nonlinearity and digitization in the field weakening region. The stator voltage space vector is calculated in the stationary reference frame using the measured DC-link voltage and the switching signals

$$\bar{v}_{s\alpha\beta} = \frac{2 * V_{DC}}{3}\left(S_a + S_b e^{j\frac{2\pi}{3}} + S_c e^{-j\frac{2\pi}{3}}\right). \tag{5}$$

Where; V_{DC} is DC-link voltage and $S_{a,b,c}$ are switching signals.

Hence, the reference stator voltage components in the stationary reference frame can be expressed as

$$\bar{v}^*{}_{s\alpha\beta} = \bar{v}_{s\alpha\beta} - \bar{\gamma}_{\alpha\beta}. \tag{6}$$

Where, $\bar{v}^*{}_{s\alpha\beta} = (v^*{}_{s\alpha} + jv^*{}_{s\beta})$ is the reference stator voltage, and $\bar{\gamma}_{\alpha\beta} = (\gamma_\alpha + j\gamma_\beta)$ is the compensating vector, which can be calculated from;

$$\bar{\gamma}_{\alpha\beta} = \left(k_{p\gamma} + \frac{K_{i\gamma}}{s}\right) * (\bar{\hat{v}}_{s\alpha\beta} - \bar{v}^*{}_{s\alpha\beta}). \tag{7}$$

Where, $k_{p\gamma}$ and $K_{i\gamma}$ are proportional and integral gains of the identical compensating controllers, respectively, and $\bar{\hat{v}}_{s\alpha\beta} = (\hat{v}_{s\alpha} + j\hat{v}_{s\beta})$ is the estimated stator voltage vector.

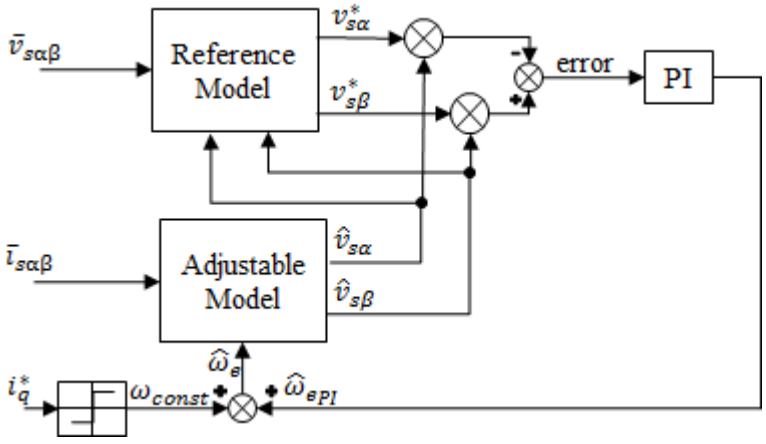

Fig. 3. Block diagram of the proposed stator voltage based MRAS scheme.

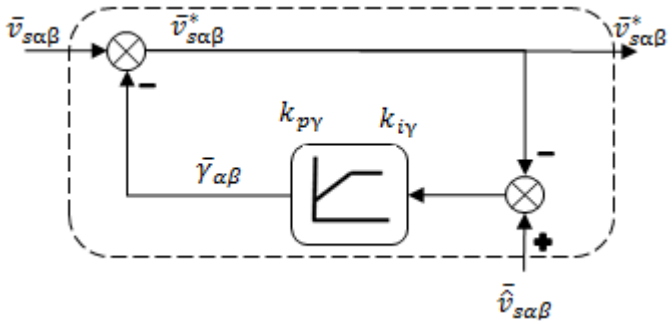

Fig. 4. Signal flow diagram of the reference model of the proposed Vs-MRAS scheme.

The signal follow diagram of the adjustable model used in this scheme is shown in Fig. 5. It uses the measured stator current components and the estimated electrical synchronous speed and in return, by mimicking the voltage model equation, calculates the estimated stator voltage components. This is derived by considering the voltage model equation of IM in the stationary reference frame as

$$\hat{\bar{v}}_{s\alpha\beta} = \hat{\bar{e}}_{m\alpha\beta} + (R_s + L_s\sigma p)\bar{\imath}_{s\alpha\beta}. \tag{8}$$

The estimated back-EMF ($\hat{\bar{e}}_{m\alpha\beta}$) is first calculated in the synchronous reference frame and then transformed into the stationary reference frame

$$\hat{\bar{e}}_{m\alpha\beta} = e_{mq}e^{j\theta_e} = (\hat{\omega}_e \frac{L_m}{L_r}\psi_{rd})e^{j\theta_e}. \tag{9}$$

Where; ($e_{mq} = \hat{\omega}_e \frac{L_m}{L_r}\psi_{rd}$) is back-EMF in the synchronous reference frame, $\hat{\omega}_e$ is synchronous speed and ($\psi_{rd} = i_d L_m$) is d-axis rotor flux.

In order to make the adjustable model independent from the term ($R_s + L_s\sigma p$), (8) can be expressed as the following:

$$\hat{\bar{v}}_{s\alpha\beta} = \left(\hat{\bar{e}}_{m\alpha\beta} + (k_1)\bar{\imath}_{s\alpha\beta}\right)k_2. \tag{10}$$

Where; first coefficient (k_1) can be treated as a known constant by setting its value to a small positive constant, e.g. in this paper for both IMs ($k_1 = 0.001$). The second coefficient (k_2), which is unknown, can conveniently be incorporated in the gains of the PI controller (adaptation mechanism). Hence, for implementing the proposed scheme the initial measured nominal values of the stator resistance and inductance, and the leakage coefficient are no longer required.

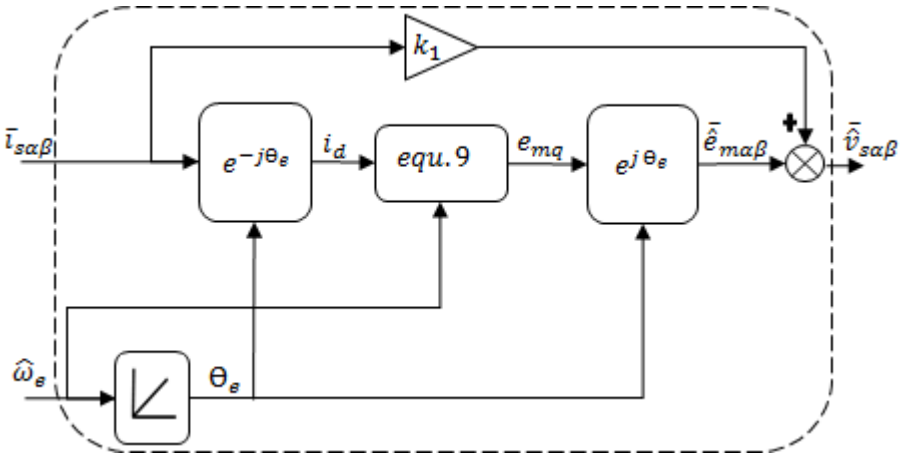

Fig. 5. Signal flow diagram of the adjustable model of the proposed Vs-MRAS scheme.

The back-EMF estimation in (9) requires synchronous speed ($\hat{\omega}_e$) which includes the estimated value of synchronous speed ($\hat{\omega}_{ePI}$), from the output of the adaptation mechanism, and a speed constant (ω_{const}).

$$\hat{\omega}_e = \hat{\omega}_{ePI} + \omega_{const}. \tag{11}$$

Where;

$$\hat{\omega}_{ePI} = \left(k_p + \frac{K_i}{s}\right) * \left(\bar{\hat{v}}_{s\alpha\beta} \otimes \bar{v}^*_{s\alpha\beta}\right). \tag{12}$$

The speed constant (ω_{const}), which is dependent on the sign of the reference q-axis current, helps the sensorless vehicle start from standstill in the correct direction that is requested by the driver.

$$\omega_{const} = \begin{cases} \omega_{const} = 1 \; for \; i_q^* > 0 \\ \omega_{const} = 0 \; for \; i_q^* = 0 \\ \omega_{const} = -1 \; for \; i_q^* < 0 \end{cases}. \tag{13}$$

Hence, utilizing the proposed scheme eliminates the requirement for slip calculation, which is normally required in IRFOC for the synchronous speed calculation and is dependent on the rotor resistance.

In order to prove the overall stability of the proposed scheme and guaranteeing that the estimated speed converges to the actual speed, the Lyapunov stability function is employed [27]. By subtracting the outputs of the reference model from the adaptive model, the error vector based on the stator voltage components can be constructed as

$$\bar{\epsilon}_{v_{s\alpha\beta}} = \bar{v}^*_{s\alpha\beta} - \bar{\hat{v}}_{s\alpha\beta}. \tag{14}$$

In order to derive the state error equations the following assumptions are made;

$$\begin{cases} x_\alpha = \dot{\omega}_e K_{\psi_d} \, sin(\theta_e) \\ x_\beta = -\dot{\omega}_e K_{\psi_d} \, cos(\theta_e). \\ \ddot{\omega}_e = 0 \end{cases} \tag{15}$$

Hence, by differentiating both sides of (14) and employing (15), the state error equations can be expressed as below;

$$\dot{\bar{\epsilon}}_{\alpha\beta} = [A][\bar{\epsilon}_{\alpha\beta}] - [W]. \tag{16}$$

Where, $\bar{\epsilon}_{\alpha\beta} = \begin{bmatrix} \epsilon_{v_{s\alpha}} \\ \epsilon_{v_{s\beta}} \\ \epsilon_{x_\alpha} \\ \epsilon_{x_\beta} \end{bmatrix}$ is the error vector, $A = \begin{bmatrix} 0 & 0 & -1 & 0 \\ 0 & 0 & 0 & -1 \\ 0 & 0 & 0 & -1 \\ 0 & 0 & 1 & 0 \end{bmatrix}$, and $W = \bar{\hat{v}}_{s\alpha\beta} \otimes (\omega_e - \hat{\omega}_e)$.

According to the Lyapunov function of the linear part in (16), the Lyapunov function (V) is selected as the following [27];

$$V = \bar{\epsilon}_{\alpha\beta}^T \bar{\epsilon}_{\alpha\beta} > 0. \tag{17}$$

Differentiating both sides of (17), we have;

$$\dot{V} = \dot{\bar{\epsilon}}_{\alpha\beta}^T \bar{\epsilon}_{\alpha\beta} + \bar{\epsilon}_{\alpha\beta}^T \dot{\bar{\epsilon}}_{\alpha\beta} = \bar{\epsilon}_{\alpha\beta}^T (A^T + A) \bar{\epsilon}_{\alpha\beta} = -I \bar{\epsilon}_{\alpha\beta}^T \bar{\epsilon}_{\alpha\beta}. \tag{18}$$

Where;

$$I = \begin{bmatrix} 0 & 0 & 1 & 0 \\ 0 & 0 & 0 & 1 \\ 1 & 0 & 0 & 0 \\ 0 & 1 & 0 & 0 \end{bmatrix} \tag{19}$$

A function is said to be asymptotically stable if the following conditions are satisfied [28]:

$$\begin{cases} 1)\ V = 0\ for\ \hat{\omega}_e = 0 \\ 2)\ V > 0\ for\ \left|\left|\hat{\omega}_e\right|\right| \neq 0 \\ 3)\ \dot{V} \leq 0 \quad \forall \hat{\omega}_e \end{cases} \tag{20}$$

Considering (17), it is clear that conditions one and two of (20) are satisfied. Moreover, (18) also satisfies the third condition in (20). Hence, it can be stated that the proposed scheme is asymptotically stable.

IV. EXPERIMENTAL SETUP

The proposed scheme was experimentally implemented and tested using a back-to-back arrangement (Dynamometer) and an electric golf buggy. The block diagram of the overall setup, its actual picture, and the golf buggy are shown in Fig. 6. The lab setup consists of a three phase 19-kW IM loaded with a surfaced-mounted permanent magnet synchronous motor (SPMSM), which both are currently used in the real automotive applications. Two 29-kW Dragon8 (D8) controllers were used for driving both motors. The D8 controllers are equipped with 32-bit floating point µ-processor, with sampling frequency of 16-kHz, and is capable of performing

four quadrant control in the speed and torque modes. The stator currents were measured using two Hall sensors, which are built in the controllers. In order to communicate with the D8 on the IM, Device Validation Tool (DVT) software was utilized. The D8 controller connected to the IM was set on the torque mode and the torque commands were applied using the DVT software on the laptop. The IM and the SPMSM were equipped with an AB and a Sine/Cos encoders, respectively. These were used for evaluation of the implemented sensorless approach. The sensorless control algorithm was hand-coded in the C-programming language and was compiled using "Keil" software development environment. The golf buggy also was equipped by a D8 and a three phase 5-kW IM. All the results were recorded using vehicle interface measurement tool, which is built in the DVT software. The nominal parameters of both IMs are provided in Appendix.

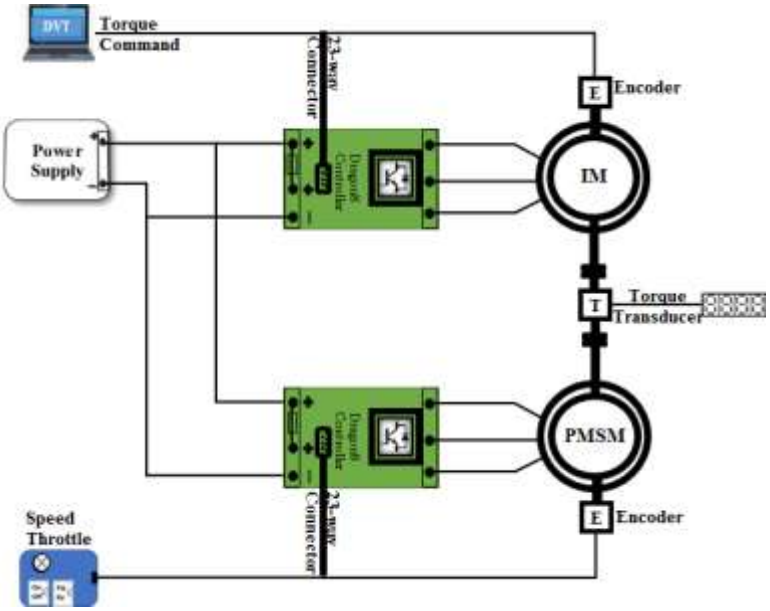

(a)

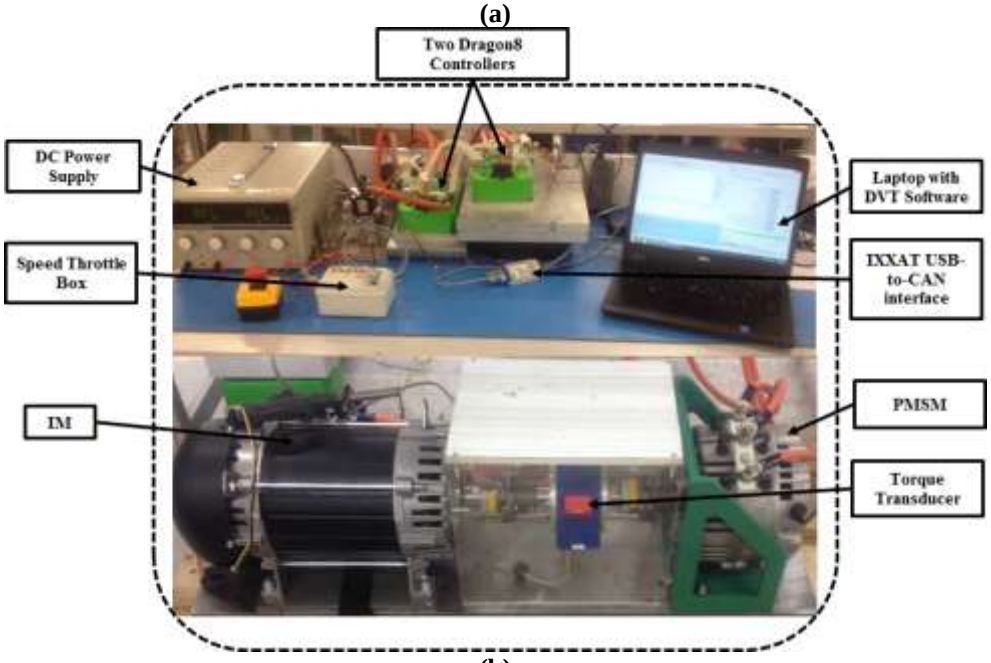

(b)

(c)

Fig. 6. Experimental setup (a) block diagram (b) actual test bench, and (c) the electric golf buggy.

V. EXPERIMENTAL RESULTS AND DISCUSSION

In this section, experimental results and discussion are presented to evaluate the effectiveness of the proposed scheme for different operating conditions. The performance of the proposed scheme is compared against that of the conventional back-EMF MRAS scheme, using Dynamometer setup. The recorded behaviours of the proposed scheme implemented on the electric golf buggy is also presented. The value of the reference d-axis stator current was produced using a LUT. All of the experiments were conducted in the sensorless mode. For the purpose of validation the estimated rotor speed has been compared against the measured rotor speed. In these tests the measured (from encoder) and estimated (from sensorless scheme) speeds were recorded using the DVT software on a laptop. The tuning procedure of PI controllers described in [15] is also used for the proposed scheme, which is as follows:

At first, the identical compensator PI controllers' gains were set to zero. Next, to obtain the optimal dynamic performance, the adaptation PI controller gains were tuned whilst the encoder signal was used for the transformation between reference frames. The proportional gain was gradually increased, while the integral gain was set to zero, until the speed from estimator could approximately track the actual speed. Then the integral gain was increased to achieve faster dynamic response. After the described procedure was carried out, both gains of the compensator PI controllers were set to one which results in a small steady state error. The error is derived to zero by gradually reducing both gains. Using the aforementioned procedure, for experiments on the dynamometer test bench, the adaptation PI controller gains of the conventional and proposed schemes were set to ($K_p = 1\ and\ K_i = 0.1$) and ($K_p = 0.5\ and\ K_i = 0.05$), respectively. The gains of the compensator PI controllers in the

reference model of the proposed scheme were set to ($k_{p\gamma} = 0.8\ and\ k_{i\gamma} = 0.001$). For experiments on the golf buggy, the adaptation PI controller gains of the proposed schemes were set to ($K_p = 0.6\ and\ K_i = 0.04$). The gains of the compensator PI controllers in the reference model of the proposed scheme were set to ($k_{p\gamma_{comp}} = 0.9\ and\ k_{i\gamma_{comp}} = 0.002$).

1. *Experimental results from Dynamometer setup*

A. Starting from Standstill with Nominal Parameters

Consistency in reliable starting from standstill with correct direction of that requested is essential in the EV applications. Therefore this test was carried out to demonstrate capability of the conventional and the proposed schemes for starting from standstill. In this test the IM was driven without load in the forward and reverse directions while the command torque of +2 Nm and -2 Nm were applied, respectively. This test was carried out in two attempts for each direction. From the result of the conventional scheme, shown in Fig. 7-(a), it is clear that, this scheme is inconsistent when starting from standstill. It can be seen that for the applied torque of -2 Nm, at 47 s, the drive became unstable and accelerated in the opposite direction to which was requested. However, from the result of the proposed scheme shown in Fig. 7-(b) it is obvious this scheme is capable of performing consistent and reliable starting from standstill in both directions.

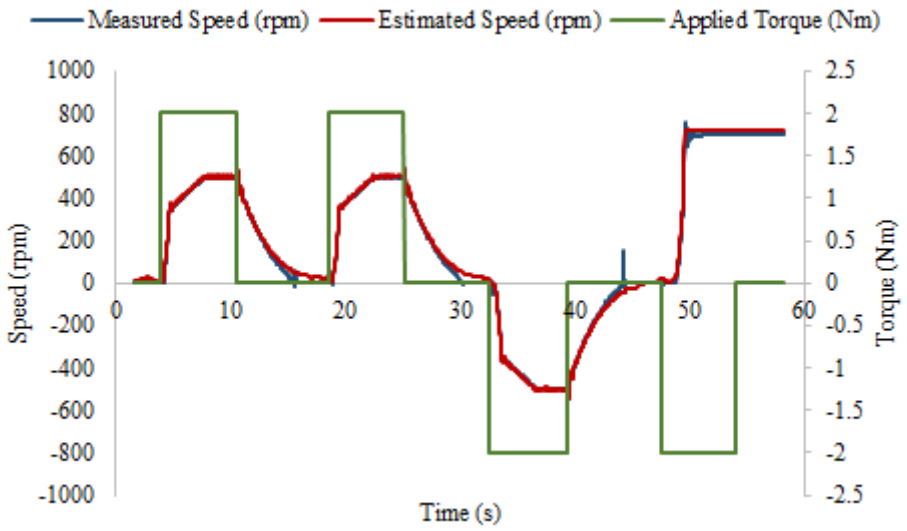

(a)

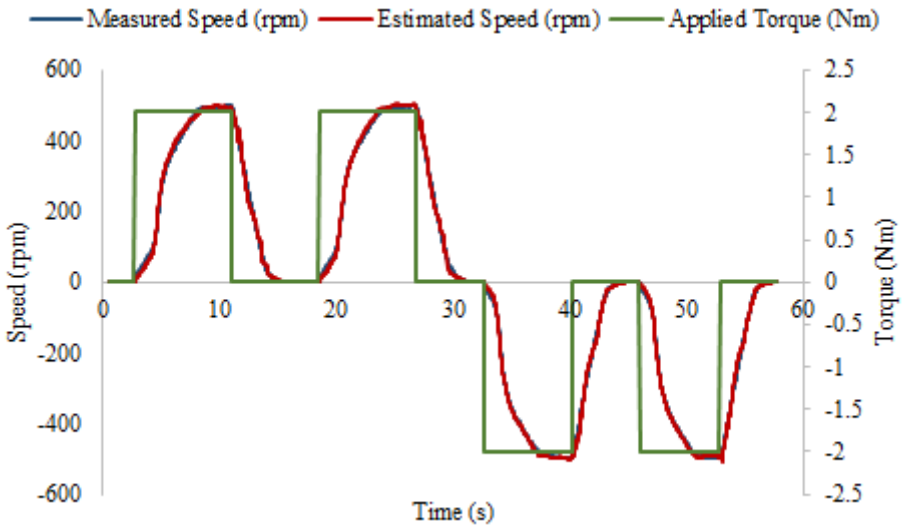

(b)

Fig. 7. Experimental results for sensorless performance starting from standstill with nominal parameters without load. (a) Conventional Back-EMF MRAS (b) the proposed Vs-MRAS

B. Sensitivity to stator resistance variation for 50% increase

This test was carried out to demonstrate the performance of the conventional Back-EMF and the proposed Vs-MRAS schemes against the stator resistance variations. In this test, for both schemes, a voltage value equal to $(0.5R_s\bar{\imath}_{s\alpha\beta})$ was added to the input voltage components of the reference model. The result of the conventional scheme is shown in Fig. 8-(a) which clearly shows that this scheme is very sensitive to stator resistance variation and become unstable in the low speed region. Fig. 8-(b) shows the result for the proposed scheme which is clear that the estimated speed closely follows the measured speed. Hence the proposed scheme is robust to stator resistance variation and performs stably in both directions.

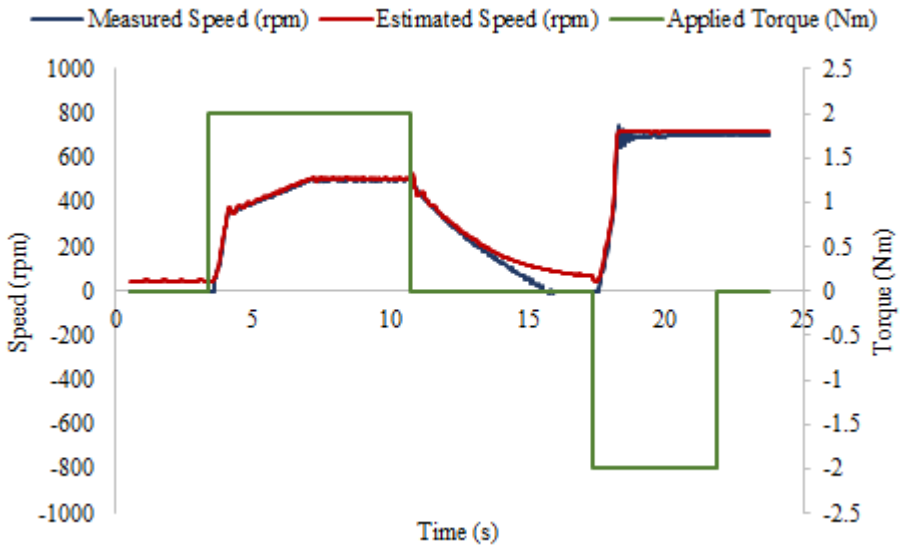

(a)

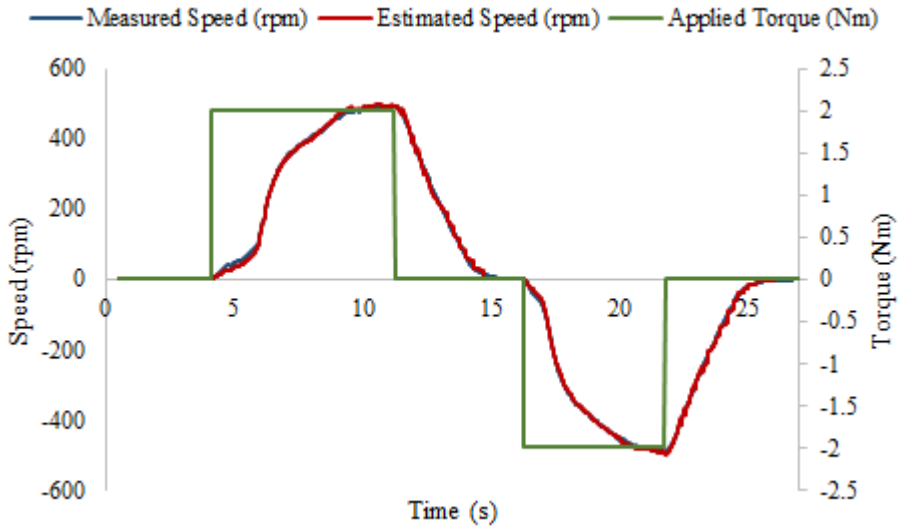

(b)

Fig. 8. Experimental results for sensorless performance with 50% increase in the stator resistance without load. (a) Conventional Back-EMF MRAS (b) the proposed Vs-MRAS.

C. Sensitivity to magnetizing inductance variation for 50% reduction

The magnetizing inductance can reduce to half of its nominal value due to the effect of saturation. Therefore, this test carried out to demonstrate the capability of the conventional and the proposed scheme while magnetizing inductance is reduced by 50% in the estimator model. During these tests the shaft speed was varied from standstill to 3000 rpm, approximately twice the rated base speed of the IM, utilizing a speed throttle connected to the SPMSM. Using both conventional and proposed scheme, a 30 Nm torque command applied from start. This test

was also carried out for the proposed scheme when compensator mechanism was not employed. The speed tracking capability of both schemes and estimated rotor flux from estimator models are shown in Figs. 9-11. Note that a moderate level of oscillations is expected when 30 Nm torque command is applied at standstill regardless of scheme used. From results of the conventional scheme, shown in Fig. 9, it can be seen that this scheme starts with excessive level of oscillations at start and completely loses control at around 2800 rpm. The performance of the proposed scheme without compensating mechanism, shown in Fig. 10, is much better than the conventional scheme, especially in the field weakening region. However, the proposed scheme without compensating mechanism has some oscillations and can become unstable during operations in the field weakening region. Although the proposed scheme with compensating mechanism, shown in Fig. 11, has some oscillations, this scheme remains stable throughout the field weakening region, twice the base speed, and also low speed regions. Hence, it can be stated that in spite of 50% magnetizing inductance the proposed scheme with compensating mechanism remains stable over a wide range of speeds, especially in the field weakening region.

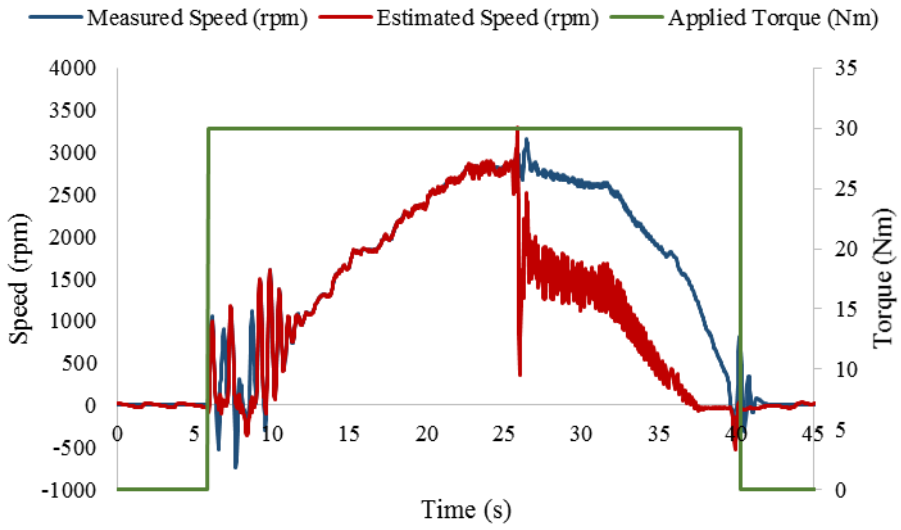

(a)

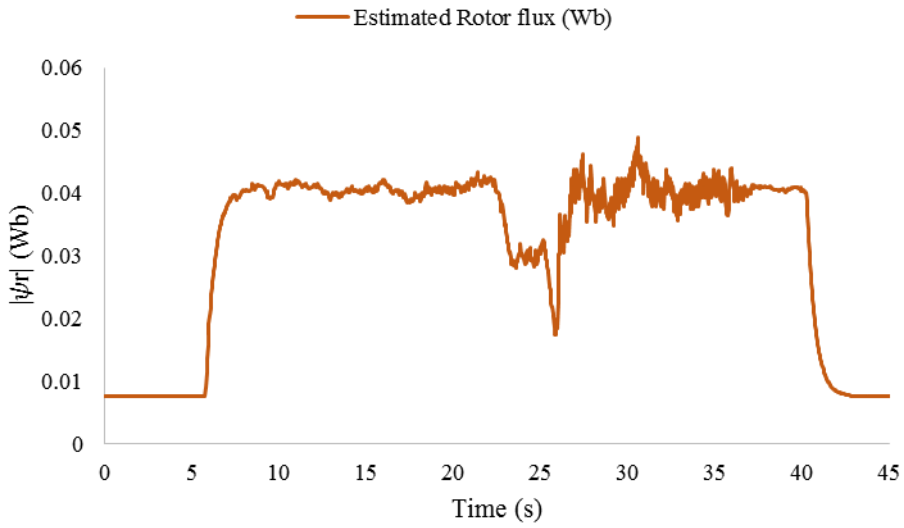

(b)

Fig. 9. Experimental result for sensorless performance using conventional Back-EMF MRAS scheme during 50% reduction in magnetizing inductance. From standstill to 3000 rpm at 30 Nm. (a) Speed tracking performance, and (b) estimated rotor flux from the estimator model.

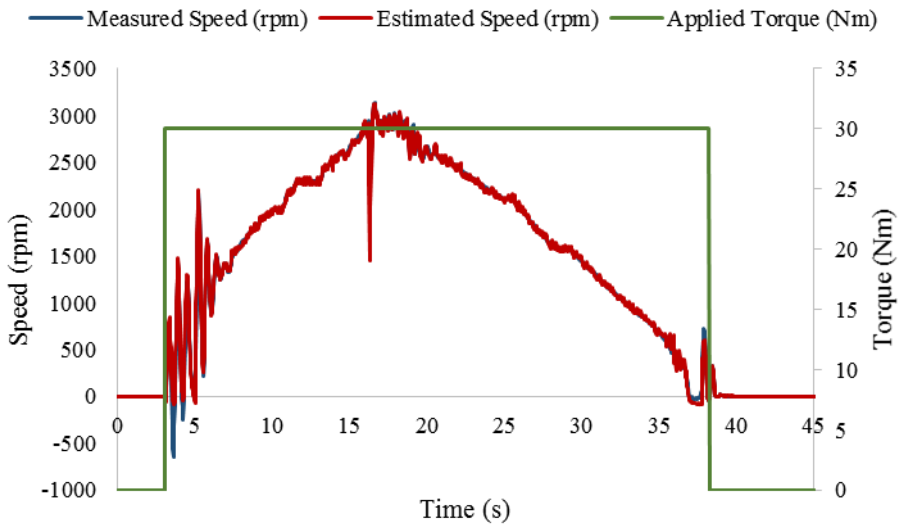

(a)

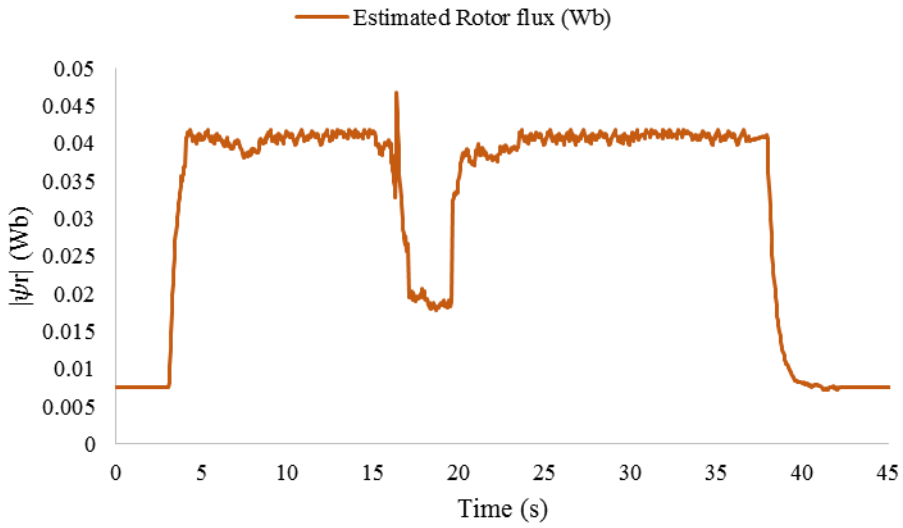

(b)

Fig. 10. Experimental result for sensorless performance using the proposed Vs-MRAS scheme without compensating mechanism during 50% reduction in magnetizing inductance. From standstill to 3000 rpm at 30 Nm. (a) Speed tracking performance, and (b) estimated rotor flux from the estimator model.

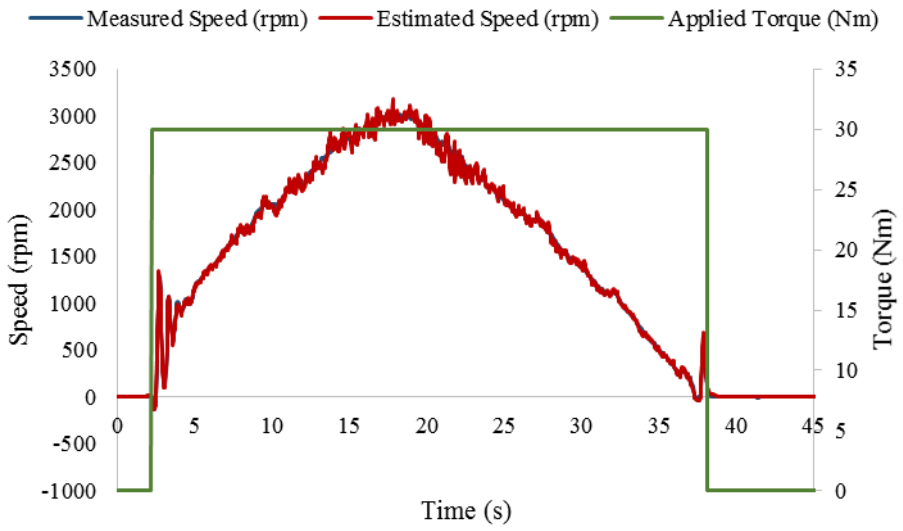

(a)

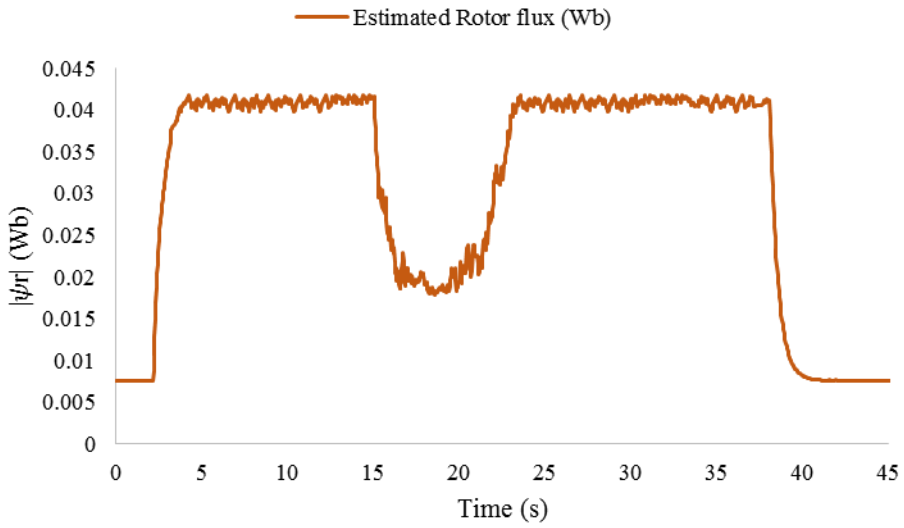

(b)

Fig. 11. Experimental result for sensorless performance using the proposed Vs-MRAS scheme, with compensating mechanism, during 50% reduction in magnetizing inductance. From standstill to 3000 rpm at 30 Nm. (a) Speed tracking performance, and (b) estimated rotor flux from the estimator model.

D. Constant speed operation with different torque levels

This test was carried out to demonstrate the behaviour of the proposed scheme at constant speed with load torque variations. For this test the shaft speed was kept constant at 400 rpm with the applied torque command varied in 5 Nm intervals from 5 Nm to 60 Nm. For this test the speed tracking capability of both schemes, and stator current components in the synchronous reference frame were recorded. Results of this test are shown in Figs. 12 and 13 for the conventional and proposed schemes, respectively. From results of the conventional scheme is clear that this scheme has significant oscillations and at 55 Nm, it completely loses stability. Hence, the estimated speed no longer tracks the measured speed. On the contrary, from results of the proposed scheme is clear that the estimated speed continuously tracks the measured speed closely regardless of variations in the torque command level.

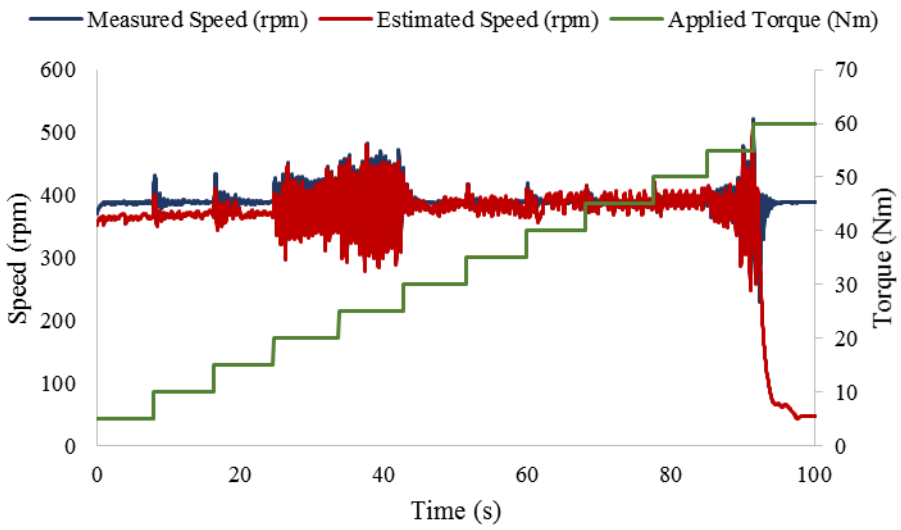

(a)

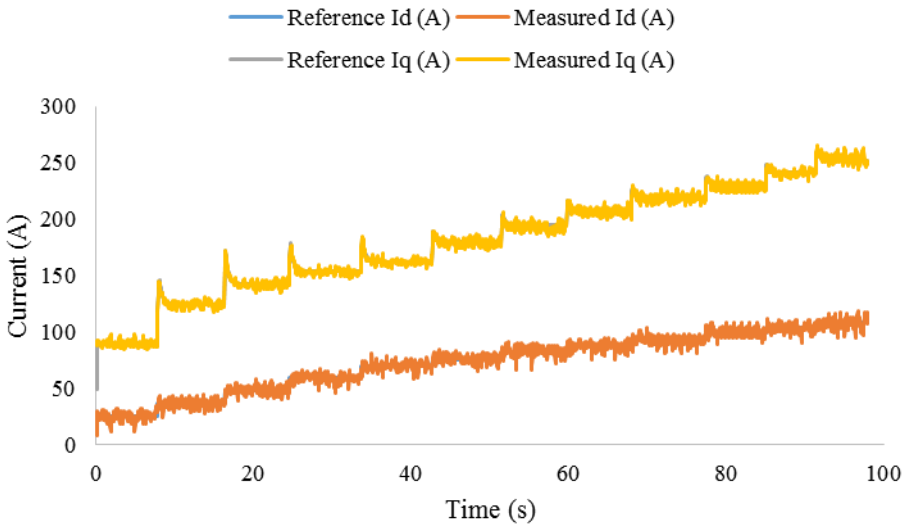

(b)

Fig. 12. Experimental result for sensorless performance using conventional Back-EMF MRAS scheme at constant speed in region of 400 rpm with the torque command increased in 5 Nm intervals from 5 Nm to 60 Nm. (a) Speed tracking performance (b) stator current components.

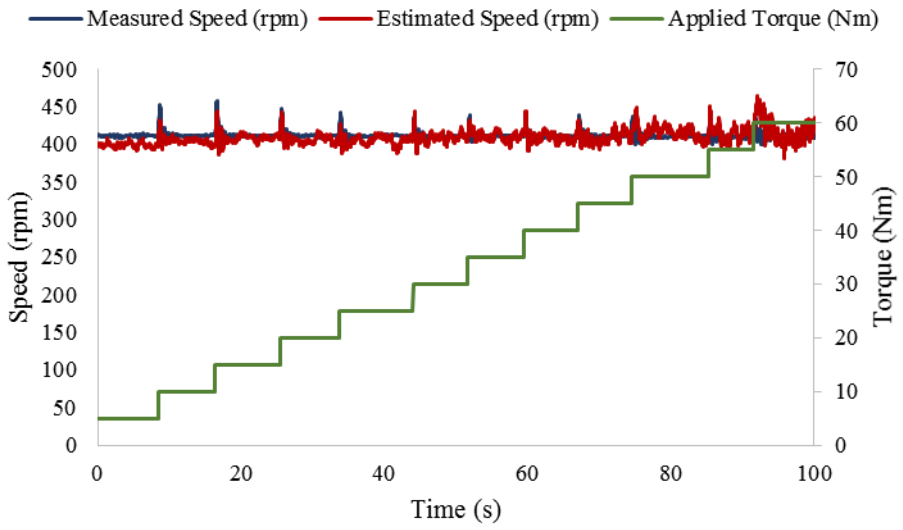

(a)

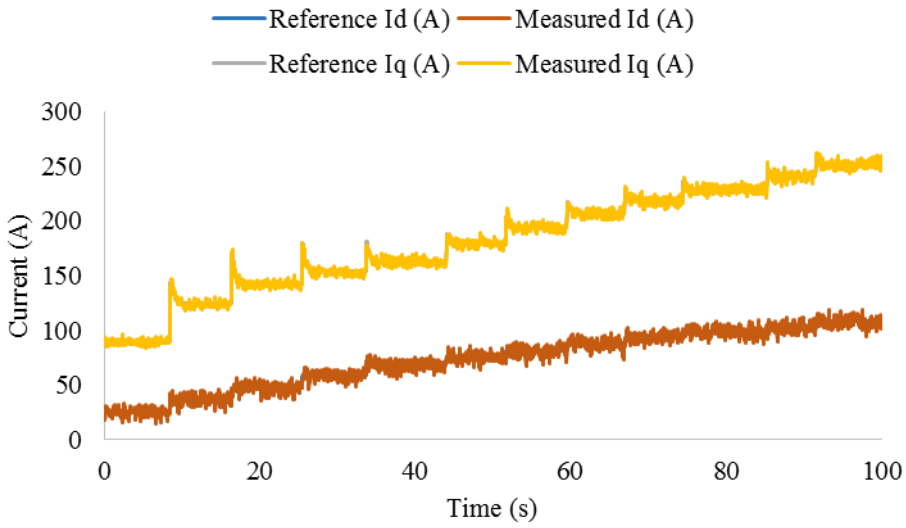

(b)

Fig. 13. Experimental result for sensorless performance using the proposed Vs-MRAS scheme at constant speed in region of 400 rpm with the torque command increased in 5 Nm intervals from 5 Nm to 60 Nm. (a) Speed tracking performance (b) stator current components.

2) Experimental results from golf buggy

The proposed scheme was implemented and tested on a golf buggy. For these tests the estimated synchronous speed, utilizing the proposed scheme, was employed in the controller. The measured speed, from encoder, was only used for validation which is labelled as “Measured Speed” in the recorded results. Results were recorded by

a laptop using DVT software. During these tests forward, park and reverse operation modes were manually selected using the vehicle's gear stick and torque command applied using accelerator pedal.

A. Consistent vehicle-starting from standstill

Consistency and reliability of the vehicle starting from standstill in the direction requested by the driver is critical when a sensorless drive employed for an EV application. Thus this test carried out to illustrate the performance of the proposed scheme for consecutive vehicle-starting in the forward and reverse operation modes. During this test the vehicle was driven in forward mode and then slowed down back to zero for three consecutive attempts. The same procedure also was repeated in the reverse direction. Vehicle test-drive result of this test is shown in Fig. 14. From the recorded result it is clear that utilizing the proposed scheme provides a consistent vehicle-starting from standstill in both forward and reverse operation modes.

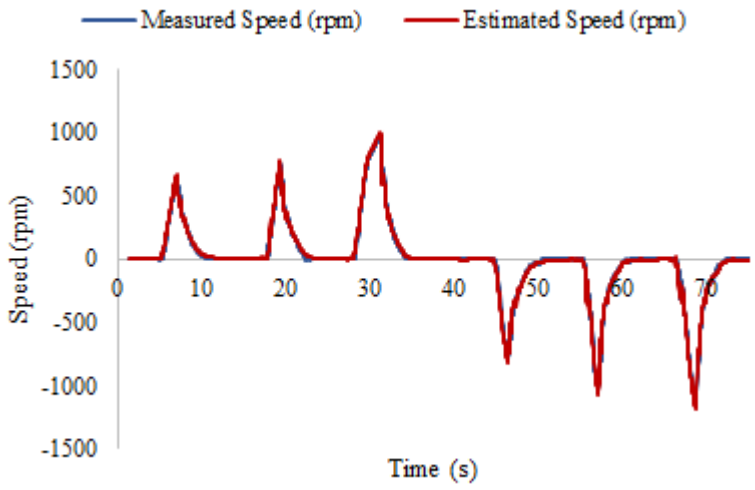

Fig. 14. Experimental results using the Golf buggy. Sensorless vehicle test-drive for 3 attempts starting from standstill in forward and reverse drive modes.

B. Smooth Forward and Reverse Test-Drive of golf buggy in wide speed range

A sensorless drive which is employed for an EV application is required to be capable of performing in wide range of speeds, including the field weakening region. Therefore this test was carried out to demonstrate behavior of the proposed scheme for the sensorless drive in forward, park and reverse operation modes in a wide range of speeds including the field weakening region. During this test the vehicle was accelerated forward to around +2950 rpm and then slowed down to zero and the same procedure was repeated for the reverse direction for the speed

around -2950 rpm. The result of this test is shown in Fig. 15, which confirms the capability and reliability of the proposed scheme across the whole speed range. The test-drive movement of the vehicle was smooth and without any cogging feelings at the vehicle-starting from standstill.

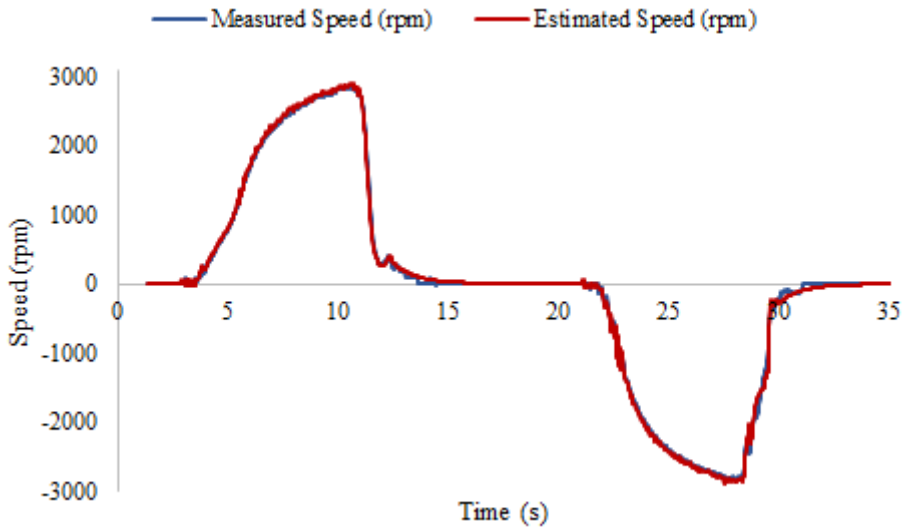

Fig. 15. Experimental results using the Golf buggy. Sensorless vehicle test-drive in forward and reverse drive modes from standstill in a wide speed range.

C. Vehicle hill-starting performance

This test was carried out to demonstrate the robustness of the proposed scheme during vehicle hill-starting test. This experiment was carried out using a 15 degree ramp, which is especially designed for hill-starting tests. This test was carried out while the vehicle was at standstill on the ramp. The result of this test is shown in Fig. 16. In order to prevent the vehicle from rolling backwards a torque command of around 4 Nm was applied, using an accelerator pedal. Then the vehicle was slowly driven forward, by gradually increasing the torque command, and slowed back to standstill by gradually easing the accelerator pedal to reduce the torque command back to around 4 Nm again. From the result it is clear that the vehicle did not roll backward while it was on the ramp and a reliable vehicle hill-starting can be achieved utilizing the proposed scheme.

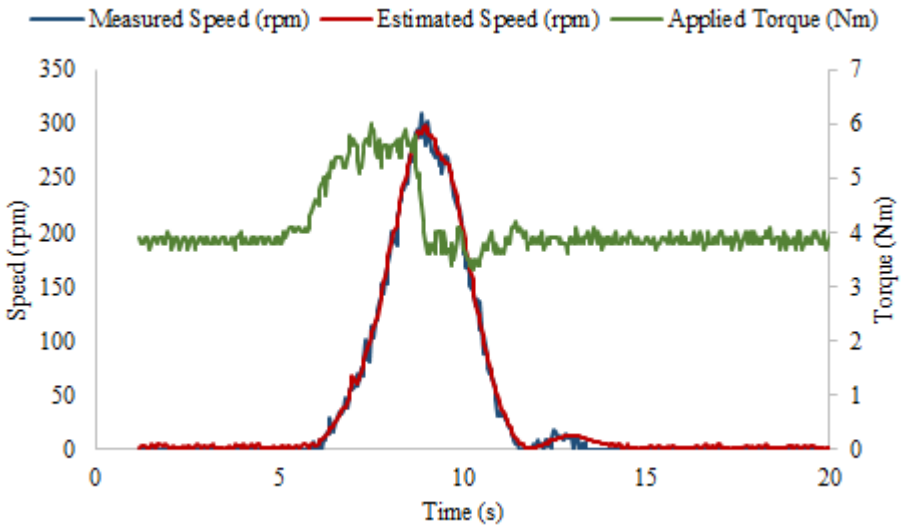

Fig. 16. Experimental results using the Golf buggy. Sensorless vehicle test-drive for hill-starting from standstill in forward mode.

VI. CONCLUSION

The proposed novel Vs-MRAS for sensorless TCD of IM for the purpose of limp-home mode of EV applications was successfully implemented in the lab environment and on an EV application (electrical golf buggy). The proposed scheme is relatively easy to implement and is independent from the prerequisite measured nominal values of stator resistance and inductance, and rotor resistance. Results of the proposed scheme confirm that this scheme is robust against parameter variations and is stable in the low speed regions. Results recorded while the proposed scheme was applied on the golf buggy confirm that a safe and consistent vehicle-starting and hill-starting from standstill can be achieved, with correct direction to that requested. More importantly, it provides a smooth and stable drive in a wide speed range, including the field weakening region. Therefore the proposed Vs-MRAS has proven to be a suitable scheme to be employed for *limp-home* mode operation in the EV/HEV applications by providing a reliable and smooth drive in a wide speed range.

APPENDIX

TABLE I. NOMINAL PARAMETERS OF IM USED IN EXPERIMENTAL SETUP

DC link voltage [V]	65	**Stator inductance [H]**	$\mathbf{7.9310 * 10^{-4}}$
Phase voltage [V] (rms)	27	**Rotor inductance [H]**	$7.9310 * 10^{-4}$
Rated torque [Nm]	48	**Rotor resistance [Ω]**	$3.1 * 10^{-3}$
Rated frequency [Hz]	52	**Stator resistance [Ω]**	$3.6 * 10^{-3}$
Rated current [A] (rms)	450	**Magnetizing inductance [H]**	$7.63 * 10^{-4}$
Number of Pole pairs	2		

TABLE II. NOMINAL PARAMETERS OF IM FOR ELECTRIC GOLF BUGGY

DC link voltage [V]	48	**Stator inductance [H]**	$\mathbf{6.18 * 10^{-4}}$
Phase voltage [V] (rms)	28	**Rotor inductance [H]**	$6.18 * 10^{-4}$
Rated torque [Nm]	22	**Rotor resistance [Ω]**	$3.045 * 10^{-3}$
Rated frequency [Hz]	78	**Stator resistance [Ω]**	$5.124 * 10^{-3}$
Rated current [A] (rms)	138	**Magnetizing inductance [H]**	$5.95 * 10^{-4}$
Number of Pole pairs	2		

References

[1] B. Akin, S. B. Ozturk, H. A. Toliyat, and M. Rayner, "DSP-Based Sensorless Electric Motor Fault Diagnosis Tools for Electric and Hybrid Electric Vehicle Powertrain Applications," *IEEE Trans. Veh. Technol.,* vol. 58, no. 5, pp. 2150-2159, 2009.

[2] M. E. H. Benbouzid, D. Diallo, and M. Zeraoulia, "Advanced Fault-Tolerant Control of Induction-Motor Drives for EV/HEV Traction Applications: From Conventional to Modern and Intelligent Control Techniques," *IEEE Trans. Veh. Technol.,* vol. 56, no. 2, pp. 519-528, 2007.

[3] D. Diallo, M. E. H. Benbouzid, and A. Makouf, "A fault-tolerant control architecture for induction motor drives in automotive applications," *IEEE Trans. Veh. Technol.,* vol. 53, no. 6, pp. 1847-1855, 2004.

[4] C. Chakraborty, and V. Verma, "Speed and Current Sensor Fault Detection and Isolation Technique for Induction Motor Drive Using Axes Transformation," *IEEE Trans. Ind. Electron.,* vol. 62, no. 3, pp. 1943-1954, 2015.

[5] D. O. Neacsu, and K. Rajashekara, "Comparative analysis of torque-controlled IM drives with applications in electric and hybrid vehicles," *IEEE Trans. Power Electron.,* vol. 16, no. 2, pp. 240-247, 2001.

[6] A. V. Ravi Teja, V. Verma, and C. Chakraborty, “A New Formulation of Reactive-Power-Based Model Reference Adaptive System for Sensorless Induction Motor Drive,” *IEEE Trans. Ind. Electron.,* vol. 62, no. 11, pp. 6797-6808, 2015.

[7] F. Alonge, T. Cangemi, F. D'Ippolito, A. Fagiolini, and A. Sferlazza, “Convergence Analysis of Extended Kalman Filter for Sensorless Control of Induction Motor,” *IEEE Trans. Ind. Electron.,* vol. 62, no. 4, pp. 2341-2352, 2015.

[8] Z. g. Yin, C. Zhao, Y. R. Zhong, and J. Liu, “Research on Robust Performance of Speed-Sensorless Vector Control for the Induction Motor Using an Interfacing Multiple-Model Extended Kalman Filter,” *IEEE Trans. Power Electron.,* vol. 29, no. 6, pp. 3011-3019, 2014.

[9] W. Sun, Y. Yu, G. Wang, B. Li, and D. Xu, “Design Method of Adaptive Full Order Observer With or Without Estimated Flux Error in Speed Estimation Algorithm,” *IEEE Trans. Power Electron.,* vol. 31, no. 3, pp. 2609-2626, 2016.

[10] H. M. Kojabadi, C. Liuchen, and R. Doraiswami, “A MRAS-based adaptive pseudoreduced-order flux observer for sensorless induction motor drives,” *IEEE Trans. Power Electron.,* vol. 20, no. 4, pp. 930-938, 2005.

[11] S. A. Davari, D. A. Khaburi, F. Wang, and R. M. Kennel, “Using Full Order and Reduced Order Observers for Robust Sensorless Predictive Torque Control of Induction Motors,” *IEEE Trans. Power Electron.,* vol. 27, no. 7, pp. 3424-3433, 2012.

[12] S. M. Gadoue, D. Giaouris, and J. W. Finch, “Sensorless Control of Induction Motor Drives at Very Low and Zero Speeds Using Neural Network Flux Observers,” *IEEE Trans. Ind. Electron.,* vol. 56, no. 8, pp. 3029-3039, 2009.

[13] Y. B. Zbede, S. M. Gadoue, and D. J. Atkinson, “Model Predictive MRAS Estimator for Sensorless Induction Motor Drives,” *IEEE Trans. Ind. Electron.,* vol. 63, no. 6, pp. 3511-3521, 2016.

[14] A. N. Smith, S. M. Gadoue, and J. W. Finch, “Improved Rotor Flux Estimation at Low Speeds for Torque MRAS-Based Sensorless Induction Motor Drives,” *IEEE Trans. Energy Convers.,* vol. 31, no. 1, pp. 270-282, 2016.

[15] E. Dehghan-Azad, S. Gadoue, D. Atkinson, H. Slater, P. Barrass, and F. Blaabjerg, “Sensorless control of IM for Limp-home mode EV applications,” *IEEE Trans. Power Electron.,* vol. PP, no. 99, pp. 1-1, 2016.

[16] J. W. Finch, and D. Giaouris, “Controlled AC Electrical Drives,” *IEEE Trans. Ind. Electron.,* vol. 55, no. 2, pp. 481-491, 2008.

[17] S. M. Gadoue, D. Giaouris, and J. W. Finch, “MRAS Sensorless Vector Control of an Induction Motor Using New Sliding-Mode and Fuzzy-Logic Adaptation Mechanisms,” *IEEE Trans. Energy Convers.,* vol. 25, no. 2, pp. 394-402, 2010.

[18] C. Schauder, “Adaptive speed identification for vector control of induction motors without rotational transducers,” *IEEE Trans. Ind. Appl.,* vol. 28, no. 5, pp. 1054-1061, 1992.

[19] F. Z. Peng, and T. Fukao, “Robust speed identification for speed-sensorless vector control of induction motors,” *IEEE Trans. Ind. Appl.,* vol. 30, no. 5, pp. 1234-1240, 1994.

[20] M. Rashed, and A. F. Stronach, “A stable back-EMF MRAS-based sensorless low-speed induction motor drive insensitive to stator resistance variation,” *IEE Proceedings -Electric Power Applications,* vol. 151, no. 6, pp. 685-693, 2004.

[21] T. Orlowska-Kowalska, and M. Dybkowski, “Stator-Current-Based MRAS Estimator for a Wide Range Speed-Sensorless Induction-Motor Drive,” *IEEE Trans. Ind. Electron.,* vol. 57, no. 4, pp. 1296-1308, 2010.

[22] M. N. Marwali, and A. Keyhani, "A comparative study of rotor flux based MRAS and back EMF based MRAS speed estimators for speed sensorless vector control of induction machines." pp. 160-166 vol.1.

[23] T. Orlowska-Kowalska, M. Dybkowski, and K. Szabat, “Adaptive Sliding-Mode Neuro-Fuzzy Control of the Two-Mass Induction Motor Drive Without Mechanical Sensors,” *IEEE Trans. Ind. Electron.,* vol. 57, no. 2, pp. 553-564, 2010.

[24] D. Casadei, F. Profumo, G. Serra, and A. Tani, “FOC and DTC: two viable schemes for induction motors torque control,” *IEEE Trans. Power Electron.,* vol. 17, no. 5, pp. 779-787, 2002.
[25] I. Boldea, M. C. Paicu, and G. D. Andreescu, “Active Flux Concept for Motion-Sensorless Unified AC Drives,” *IEEE Trans. Power Electron.,* vol. 23, no. 5, pp. 2612-2618, 2008.
[26] I. M. Alsofyani, and N. R. N. Idris, “Simple Flux Regulation for Improving State Estimation at Very Low and Zero Speed of a Speed Sensorless Direct Torque Control of an Induction Motor,” *IEEE Trans. Power Electron.,* vol. 31, no. 4, pp. 3027-3035, 2016.
[27] I. Benlaloui, S. Drid, L. Chrifi-Alaoui, and M. Ouriagli, “Implementation of a New MRAS Speed Sensorless Vector Control of Induction Machine,” *IEEE Trans. Energy Convers.,* vol. 30, no. 2, pp. 588-595, 2015.
[28] G. F. Franklin, J. D. Powell, and A. Emami-Naeini, *Feedback Control of Dynamic Systems*, 6th ed., pp. 654-660, Upper Saddle River: Pearson Education, 2010.